[2] Ashish Ravalia, Bharat Kataria, SavanKatba, Sadaf Jethva, MeghaVagadia, K. Asokan, Sanjeev Gautam, Keun Hwa Chae, D.G Kuberkar, Vacuum **155**, 572—577(2018).

5.2.51 A reversible tuning of fermi level in $BiSbTe_3$ thin films through ion implantation

Jyoti Yadav[1], Anoop M D[1], Rini Singh[2], Nisha Yadav[1], N. Srinivasa Rao[1], Fouran Singh[3], Ankur Jain[2,5], Takayuki Ichikawa[4], Kamlendra Awasthi[1], and Manoj Kumar[1]

[1]*Department of Physics, Malaviya National Institute of Technology Jaipur, Rajasthan, 302017, India*
[2]*Graduate School of Engineering, Hiroshima University, Higashi-Hiroshima, 739-8527, Japan*
[3]*Inter-University Accelerator Centre (IUAC), New Delhi - 110067, India*
[4]*Natural Science Centre for Basic Research and Development, Hiroshima University, Higashi-Hiroshima, 739-8530, Japan*
[5]*Centre for Renewable Energy and Storage, Suresh Gyan Vihar University, Jagatpura, Jaipur-302017, India*

In order to control critical electronic and physical properties using control over implantation-induced strain, we have fabricated bismuth antimony telluride thin films ($BiSbTe_3$) through electron-beam deposition technique. [*for details, see Mater. Lett. 306 (2022) 130923*]. The influence of Fe-Implantation at Sb site of $BiSbTe_3$ on the structural and electrical properties was investigated via various characterization techniques such as, X-ray Diffraction and Hall Effect measurements. The XRD spectra reveal the rhombohedral layered structure of the samples in the R3m space group. The effect of Fe ion implantation on the structural properties of $BiSbTe_3$ thin films suggests the dynamic control over strain. A reversibly tuned strain in thin films indicate the application of thin films in control switching devices where charge carriers are controlled using internal strain. The temperature dependent resistivity measurements in temperature range 4-300 K show that the vacancies created and distribution of ions by implantation induced defects plays significant role in transport properties. The implantation of Fe ions resulted enhancement in semiconducting nature of thin films. In the case of $BiSbTe_3$ donor type defects dominates over hole type defects. The decrease in resistivity for the higher fluences is due to the donor defects induced by Fe implantation. The total resistivity is found to be composed of 3 types of conduction behavior. The crossover from variable range hopping (VRH) to activation behavior is observed in resistivity. In the mid-temperature range (35 K < T < 135 K), it follows the 3D VRH mechanism ($\rho_{xx} \propto \exp(T/T_0)^{-1/4}$). T_0 is the characteristic temperature and it changes with the presence of defects and disorders. Similarly, the resistivity of thin films also follows activation behavior in the high-temperature range (135 K <300 K). It is assumed that local annealing reduces the crystalline defects and vacancies which decrease the carrier concentration as well as enhance the activation energy (Δ) of the material from 3.68 eV for pristine to 7.82 eV for $1x10^{13}$. The Hall Effect measurements was carried out at fixed magnetic field of 0.25 T. The value of the Hall coefficient indicates the nature of charge carriers and the position of the Fermi energy level. It has been observed implantation-induced defects enhance the temperature dependency of Hall charge carriers. The thermally activated transition from *p*-type to *n*-type is observed at a temperature around 130 K for the higher fluence. The Hall Effect measurements revealed reversible tuning of Fermi level by Fe implantation in $BiSbTe_3$.

In order to investigate the effects of the transition metal ion implantation on the structural and electrical properties, the Sb_2Te_3 thin films were deposited on SiO_2/Si wafer using electron beam evaporation technique at MNIT, Jaipur. The distance between the target and substrate was adjusted at 5 cm and the power during the deposition was kept at 5W. These films have been deposited in high vacuum of order 10^{-6} mbar. During the deposition substrate temperature was maintained at room temperature and all the films were deposited for 30 minutes. After phase analysis the films were implanted using SNICS negative ion implanter at Inter University Accelerator Centre (IUAC), New Delhi with Fe 100 keV ions at three different ion fluences i. e. 1×10^{13} ions/cm^2, 1×10^{14} ions/cm^2 and 5×10^{14} ions/cm^2 with current of 10 μA. [*for details, see Macromol. Symp. 399 (2021) 2100079*]. All the films were fixed to the target ladder placed inside the high vacuum (~10^{-6} torr) chamber during implantation. To investigate the structural changes because of the implantation, we have carried out the XRD measurements of the implanted thin films at room temperature at Hiroshima University, Japan. To investigate the modifications in band structure, low-temperature transport studies were carried out. The temperature-dependent resistivity measurements in the temperature range (4 K-300 K) suggests the semiconducting nature of thin films. [*for details, see Appl. Phys. A. 127 (2021) 5130*]. At lower temperatures, longitudinal resistivity (ρ_{xx}) showed an upturn which is due to the disordering in the films, electron-electron interaction (EEI), or Weak Antilocalization (WAL) effects.

REFERENCES:

[1] Jyoti Yadav, Anoop M D, Rini Singh, Nisha Yadav, N. Srinivasa Rao, Fouran Singh, Ankur Jain, Takayuki Ichikawa, Kamlendra Awasthi, and Manoj Kumar, Mater. Lett. **306**, 130923 (2022).

[2] Jyoti Yadav, Anoop M D, Rini Singh, Nisha Yadav, N. Srinivasa Rao, Fouran Singh,Takayuki Ichikawa,Ankur Jain, Kamlendra Awasthi, and Manoj Kumar, Macromol. Symp. **399**, 2100079(2021).

[3] Jyoti Yadav, Anoop M D, Rini Singh, Nisha Yadav, N. Srinivasa Rao, Fouran Singh, Kamlendra Awasthi, and Manoj Kumar, Appl. Phys. A. **127,** 5130(2021).

5.2.52 Study of sub-band states formation in the optical band gap of $CuGaS_2$ thin films by electronic excitations

S. Suba Viveka[a], T. Logu[b, f], N. Ahsan[b], K. Asokan[c], S. Kalainathan[d], K. Sethuraman[a, e]*, and Y. Okada[b]

[a] *School of Physics, Madurai Kamaraj University, Madurai, Tamil Nadu, India*
[b] *Research Center for Advanced Science and Technology (RCAST), The University of Tokyo, Tokyo, Japan*
[c] *Materials Science Division, Inter-University Accelerator Centre (IUAC), New Delhi, India*
[d] *Centre for Nanotechnology Research, Vellore Institute of Technology, Vellore, India*
[e] *Department of Materials Science, School of Technology, Central University of Tamil Nadu Thiruvarur, India*
[f] *SPECIFIC, Materials Research Centre, Faculty of Science and Engineering, Swansea University, Swansea, UK*

Solar cells have emerged as one of the most trending energy resources used worldwide. In this work, a chalcopyrite system $CuGaS_2$ is extensively used for the study of photovoltaic applications due to its low toxicity, direct optical band gap, and high absorption coefficients. Swift heavy ion (SHI) irradiation is effectively used to determine the better photo-absorber material for photovoltaic applications. Different materials like Au, Ag and O ions are employed in SHI irradiation at higher energies to investigating the structural, optical, morphological and electrical properties. Pristine CGS thin film was deposited onto a substrate using Chemical Spray Pyrolysis (CSP), with a coating temperature of 220 °C. Further, irradiation with 120 MeV Au and Ag ions and 100 MeV O ions with fluences of 5 x 10^{12} ions/cm^2. Powder XRD analysis revealed the intensity of the dominant peak in pristine CGS was reduced after irradiation of O and Ag ions which is due to the defects generated by the ions. The crystallite size measured was found to be increasing since SHI irradiation from pristine CGS. Micro Raman analysis provided the evidence supporting the XRD analysis, with significant crystallite size upon irradiation. UV/Vis-NIR analysis provided information about the formation of sub-band-gap in the irradiated CGS where a redshift was observed at 680nm compared with pristine CGS at 510nm.

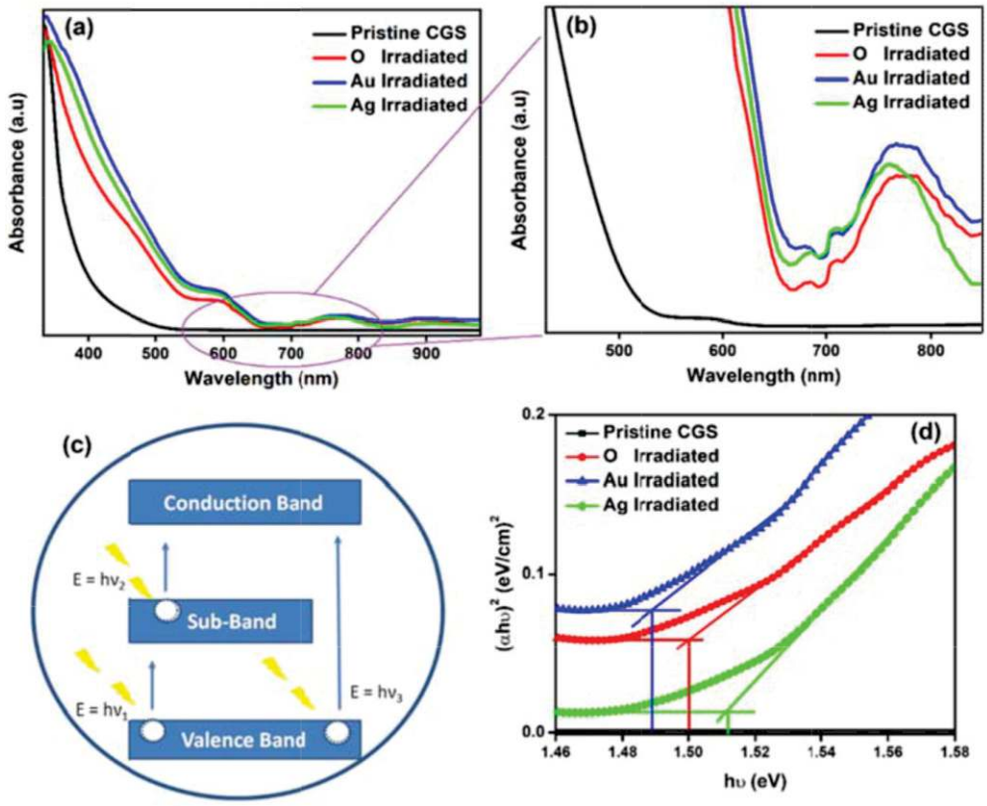

Fig. 1. (a) UV/Vis-NIR spectra of pristine and SHI-irradiated CGS thin films; (b) magnified view of the circled region; (c) schematic sketch of sub-band optical transitions; (d) Tauc plot of sub-band optical response.

Morphological studies such as AFM showed the increment of grain size after SHI irradiation from pristine CGS. SEM analysis revealed Nano-flake grains observed in pure CGS which happened to grow upon SHI irradiation, enhancing the electrical and optoelectrical properties. EDAX was used to confirm the presence of Cu, G and S. The electrical/Hall studies showed the decrease in resistivity of the film after irradiation due to the increased ion mobility. The photosensitivity of the films was determined and that of Au ion irradiated CGS thin film showed a better result of about 7.82 providing enhanced carrier concentrations upon SHI irradiation. With these experimental studies and analysis of the results, we conclude that SHI irradiation is an effective process for enhancing the electrical and optoelectrical properties which can be very well utilized in Photovoltaic applications.

REFERENCES:

[1] S.S. Viveka, T. Logu, N. Ahsan, K. Asokan, S. Kalainathan, K. Sethuraman, Y. Okada, Study of sub-band states formation in the optical band gap of CuGaS2 thin films by electronic excitations, J. Phys. Chem. Solids. 164, 110636(2022).

5.2.53 Enhancement of Photoelectric properties of Cu_2ZnSnS_4 thin films by electronic excitations induced by swift heavy ions

M. Sampath[a,e] T. Logu[a,f], P. MathanKumar[b], K. Asokan[c], and K. Sethuraman[d,*]

[a] *School of Physics, Madurai Kamaraj University, Madurai, Tamil Nadu, India*
[b] *Department of Energy, University of Madras, Guindy Campus, Chennai, Tamil Nadu, India*
[c] *Inter University Accelerator Centre (IUAC), New Delhi, India*
[d] *Department of Materials Science, School of Technology, Central University of Tamil Nadu, Thiruvarur, Tamil Nadu, India*
[e] *Syed Ammal Arts and Science College, Ramanathapuram, Tamil Nadu, India*
[f] *SPECIFIC, Materials Research Centre, Swansea University, Swansea, UK*

Solar cells are prominent devices to exploit renewable energy resources. Copper Zinc Tin Sulfide (CZTS) is preferable absorber material to other toxic and scarce materials. The existence of secondary phases and defects are the factors affecting its efficiency to reach the SQ limit. In this report, Swift Heavy Ions (SHI) were irradiated to reduce the above factors. The transparent precursor solution of CZTS was coated on the substrate at 350°C by the spray pyrolysis method. Pristine and irradiated samples have a thickness of about 1.2 m. CZTS thin films were irradiated with 120 MeV Au ions and 100 MeV Ag and O ions with a fluence of 5 x10^{12} ions per cm^2. Electronic energy loss, nuclear energy loss and projectile range were calculated by SRIM software. The collision events, energy loss to target phonon, Ion recoil distribution, energy to recoils, and ionization recoils were investigated by TRIM software. Crystallite size of the Ag and O irradiated samples were increased but in kind of Au irradiated films was decreased. Ag and O irradiation improved structural properties. Micro Raman results replicated that lattice defects in Au irradiated samples and the highest peak confirms A symmetry mode of Kesterite structure.

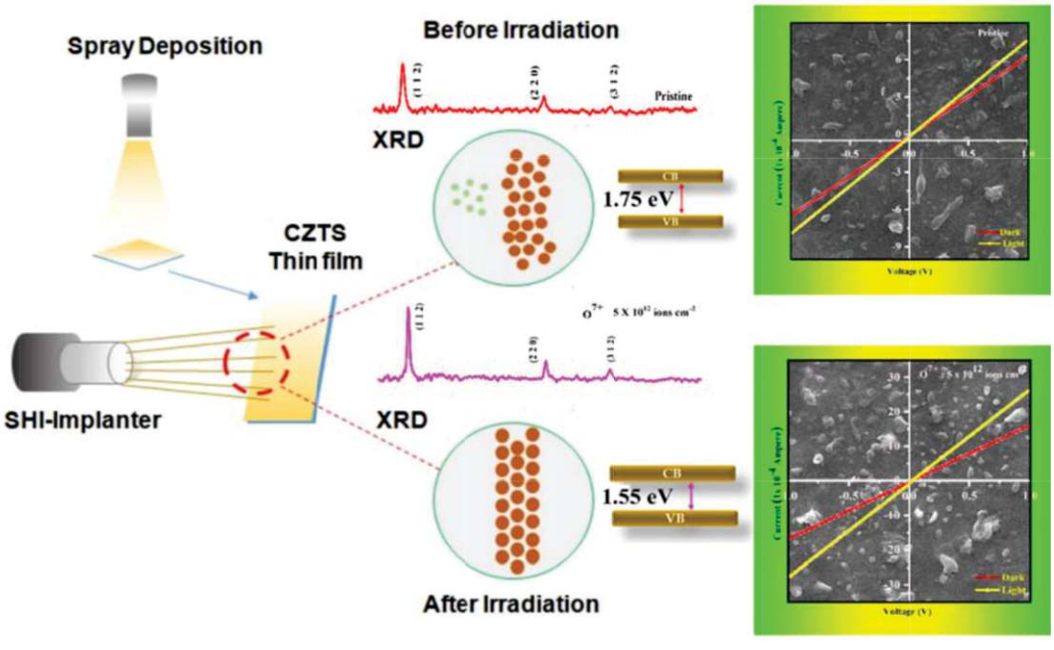

Fig. 1 Schematic diagram illustrates the SHI induced modifications in CZTS

Surface morphology of the samples was carried out by SEM and variations in the particle size were correlated with XRD and Raman results. Chemical compositions were confirmed with EDS and XPS results. The optical properties of O irradiated film showed high absorbance and lower optical bandgap than other films. Irradiation significantly increases the photoelectric properties of the Ag ad O irradiated sample. Maximum photosensitivity of 62% was obtained for O irradiated sample. Eventually, the effects of irradiation in CZTS thin films were reflected in structural, and optical properties, especially in photoelectric properties. So irradiated CZTS thin films are suitable for optoelectronic applications.

REFERTENCES:

[1]M. Sampath, T. Logu, P. Mathan Kumar, K. Asokan, K. Sethuraman, Enhancement of photoelectric properties of Cu2ZnSnS4 thin films by electronic excitations induced by swift heavy ions, Mater. Sci. Eng. B. 280, 115683(2022).

5.2.54 Irradiation induced interface and magnetic study of Zinc ferrite/insulator/ cobalt ferrite multilayers

Shaffy Garg[a] , Sanjeev Gautam[a,*], Ramcharan Meena[b], Navdeep Goyal[c]

[a]*Advanced Functional Materials Lab., Dr. S. S. Bhatnagar University Institute of Chemical Engineering & Technology, Panjab University, Chandigarh, 160 014, India*
[b]*Materials Science Division, Inter-University Accelerator Centre, New Delhi - 110 067, India*
[c]*Department of Physics, Panjab University, Chandigarh 160 014, India*

Magnetic tunnel junction (MTJ) has a significant role in the development of spintronic devices. MTJ contains two FM layers separated by a tunnel barrier influenced by perpendicular magnetic anisotropy and spin-transfer torque which are governed by interface structural properties. An electrical current passing through pair of FM electrodes separated by a tunnel barrier exerts pseudo-torque on the magnetic moment of the individual electrodes, which is proportional to the electrical current. Past efforts observed the interface assembly of MTJ by bearing in mind Fe/MgO/Fe and Fe/NaCl/Fe structures. The magnet direction of two FM layers can be controlled by an applied magnetic field separately. If the spin orientations of two FM layers are parallel, it is easier for electrons to tunnel through the barrier than in an antiparallel state. Therefore, the resistance of the junction shows two states, which is known as tunnel magnetoresistance (TMR). Spin polarization of FM layers is a major cause of TMR of MTJ. A high TMR ratio in MgO-based MTJs requires correct crystalline orientation of the FM electrodes and lattice matching at the interfaces between the electrodes and the tunnel barrier. This article discusses the design of ferrite-based multilayers and magnetic tunnel junctions with their interface properties [1]. This research includes the synthesis and characterization of oxide multilayers for MTJ application (IUAC/XII.3A/Jan 12, 2018).

REFERENCES:

[1] Design of ferrite-based magnetic tunnel junction, Shaffy Garg, Jatinder Pal Singh, Keun Hwa Chae, K. Asokan, Navdeep Goyal, Sanjeev Gautam" to the Elsevier book entitled "Ferrite nanostructured magnetic materials: Technology and Applications" (isbn:9780128237182) Edited by J.P. Singh *et. al*.

5.2.55 Characterizing the defects and ferromagnetism in metal oxides: The case of magnesium oxide

Shaffy Garg[a] , Sanjeev Gautam[a,□], Jitendra Pal Singh[b], Kandasami Asokan[c], Navdeep Goyal[d]

[a]*Advanced Functional Materials Lab., Dr. S. S. Bhatnagar University Institute of Chemical Engineering & Technology, Panjab University, Chandigarh, 160 014, India*
[b]*Beamline Division, Pohang Accelerator Lab, POSTECH, South Korea*
[c]*Materials Science Division, Inter-University Accelerator Centre, New Delhi - 110 067, India*
[d]*Department of Physics, Panjab University, Chandigarh 160 014, India*

Defects play an essential role in controlling the phenomenon of d0 ferromagnetism in nonmagnetic oxides. Defects can have a significant impact on behavior, especially d0 ferromagnetism of oxide materials at room temperature (RT). Defects in magnesium oxide can be created by various phenomena like ion implantation, swift heavy ion/laser/gamma or UV irradiation, etc. [1]. This review focuses on the various characterization tools that are helpful to identify the nature of defects in the materials. Microscopic studies infer the crystal structure modification via doping concentrations in metal oxides. Tools like ultra-violet visible (UV–Vis) spectroscopy and photoluminescence (PL) spectroscopy enrich the information on defects as well as depict the kind of vacancy. Electron paramagnetic resonance (EPR) is suitable to get information on spin centers in the materials. In addition to this, synchrotron radiation-based techniques like X-ray absorption spectroscopy (XAS), and X-ray magnetic circular dichroism (XMCD) is also helpful to know about the structural defects and nature of vacancy in the materials [2]. Vibrating sample magnetometry (VSM)/superconducting quantum interference device (SQUID) measurements deduce the magnetic properties and cause of the ferromagnetism in the metal oxide. Thus, these characterization tools are covered in this review by addressing the origin of defects as well as the methodology utilized to create and control defects in the materials. The IUAC project for beamtime utilization (UFR-63323) is duly acknowledged along with IUAC collaborator Dr. K. Asokan [1].

REFERENCES:

[1] Characterizing the defects and ferromagnetism in metal oxides: The case of magnesium oxide, Shaffy Garg, Sanjeev Gautam, Jitendra Pal Singh, Kandasami Asokan, Navdeep Goyal Material Characterization**, 179**, 111366(2021).

[2] Electronic structure of Fe/MgO/Fe multilayer stack by X-ray magnetic circular dichroism, Sanjeev Gautam, Kandasami Asokan, Jitendra Pal Singh, Fa-Hsiu Change, Hong-Ji Lin, and Keun Hwa Chae, J. Appl. Phys., **115**, 17C109 (2014).

5.2.56 A study of structural and electrical properties of tetravalent metal doped α- Fe_2O_3 systems

Divya Sherin GT[1], R. N Bhowmik[1*], A Tripathi[2], Sanjay Kumar Kedia[2], R.C Meena[2], and S.A Khan[2]

[1]*Department of Physics, R.V Nagar, Pondicherry University, Kalapet-605014, India.*
[2]*Material Science Group, Inter-University Accelerator Centre, Aruna Asaf Ali Marg, New Delhi-110067, India*

In the search for corundum structured metal oxides having magneto-electric properties for applications in low power spintronic devices, Hematite (α- Fe_2O_3) has been selected here as the basic system and tetravalent elements [1], such as Si, Ge and Sn have been doped to enhance the electrical conductivity. The nanocrystalline (bulk) materials were prepared by mechanical milling and chemical co-precipitation routes. GIXRD, FE-SEM, EDX, R-T measurements and Thermal evaporation technique for thin film preparation at IUAC were used. The as-prepared nanocrystalline powders with compositions ($Fe_{1.952}TE_{0.048}O_3$, where TE=Si, Ge, Sn) were heated in air at 550°C to stabilize the rhombohedral phase and confirmed by XRD (2 =20°-80°) at 300 K. A small amount of unreacted SnO_2 was found for Sn-doped α- Fe_2O_3 composition. Surface morphology of the samples were studied using SEM images (TESCAN's MIRA II LMH), as shown in figures below.

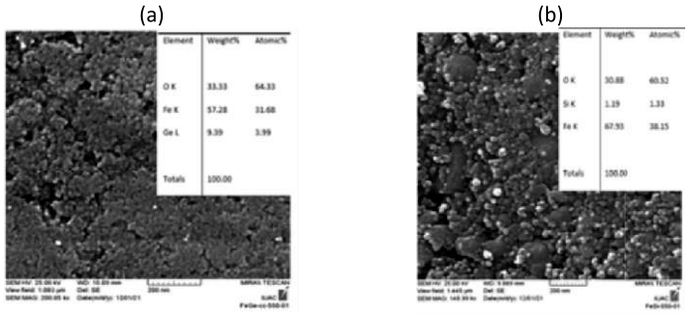

Figure. SEM image of the (a) FeGe-CC and (b) FESi pellet samples. The corresponding composition calculated from EDX are shown as insets.

Particle size was calculated for as-prepared and annealed samples from SEM images using ImageJ software and found in the range of 3-14 nm. Nanoparticles exhibit irregular shape but evenly distributed in FeSi and FeGe-MM samples, while coagulation of particles (like a sheet of uniform distribution) is seen in FeGe-CC samples and FeSn sample exhibits clustering of nanoparticles. The elemental composition of the samples was determined using EDX (model Oxford Instruments' INCA PENTA FET3). The EDX spectra revealed the doping at 6.8%, 5.9%, 24.5%, 3.97% in FeSi (Si doped Fe_2O_3), FeGe-MM, FeGe-CC (MM-mechanical milled, CC-chemical coprecipitation), FeSn respectively. Resistance (R-T) of the samples were measured in a narrow temperature range of 320K-420K due to the fact high resistance of the samples. The R-T plots showed that conductivity has been significantly enhanced of the order of $10^{-2}\Omega^{-1}m^{-1}$ and $10^{-3}\Omega^{-1}m^{-1}$ for FeGe-MM-A550 and FeSi-A550 (both air annealed at 550°C), respectively, while other samples exhibited conductivity in the range of $10^{-4}\Omega^{-1}m^{-1}$ to $10^{-6}\Omega^{-1}m^{-1}$. Also, the thin films of pure Fe and Si-doped Fe_2O_3 system were grown on p-Si(100), Quartz and Al_2O_3 substrates using thermal evaporation method. The crystalline structure is not clear in the as-grown films from XRD measurements. However, heat treated Fe and Si-doped Fe_2O_3(FeSi) films at 800°C for 7 hours showed crystalline structure of hematite phase.

REFERENCES:

[1] Peilin Liao, Maytal Caspary Toroker, Emily A.Carter, Nano Lett., **11**, 1775–1781(2011).

5.2.57 Surface morphology and microstructural studies of Cu doped CdS QDs

Tania Kalsi and Pragati Kumar

Department of Nanosciences and Materials, Central University of Jammu, Rahya Suchani, Samba-181143, J&K, India

In order to study the surface morphology, elemental analysis, crystalline structure and size, and microstructural defects present in Cu doped CdS QDs FE-SEM, EDX, TEM, HRTEM and SAED analysis were carried out at IUAC, New Delhi. Fig. 1. shows the FE-SEM images and EDX of undoped and 3% Cu doped CdS QDs. Fig. 1(a) depicts the densely packed grain distribution which resembles the coral reef-like structures for the pure CdS with tightly bound of the particles forming clusters while there is segregation of the particles in the Cu doped CdS nanoparticles. The inset of the fig. 1(b) shows the magnified images of the particular surfaces (i), (ii) and (iii). These surfaces show the loosely bound large particles which perfectly correlate with TEM images as described in the next section. The qualitative elemental analysis was carried out through EDX to study the elemental distribution in CdS and 3 wt% Cu

doped CdS samples. The analyzed positions in the sample are given in Fig. 1 (c) and (d) for undoped and doped CdS respectively. In Fig. 1 (d) peaks relate to Cd, Cu and S confirm that the impurity element was incorporated in CdS nanoparticles. It can be seen from Fig.1 (c) and (d) that the Cd and S in CdS & Cd, Cu and S in $Cd_{0.97}Cu_{0.03}S$ are well-distributed throughout the sample.

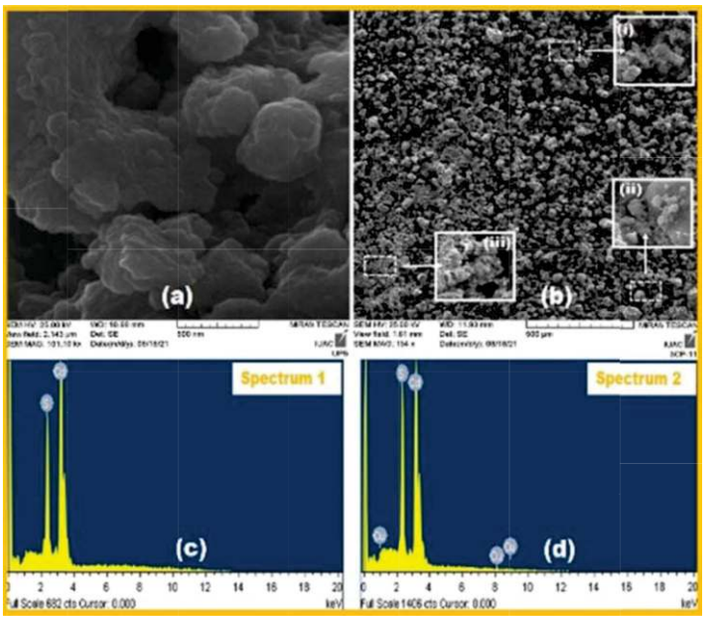

Fig. 1(a) and (b) SEM images, (c) and (d) EDX spectra of undoped and 3 at% Cu doped CdS QDs

TEM studies were performed to highlight the shape, size, size distribution and defects in pure and Cu doped CdS NPs. For this purpose, a clear solution of undoped and 3% Cu doped CdS NPs in DMSO is prepared by ultrasonication of solution for 1 h. A few drops of the solution were placed on the carbon coated copper grid for TEM characterization.

Fig 2(a) and (b) represents the TEM micrograph of pure and Cu doped CdS NPs respectively. TEM images show that spherical morphology and cluster formation in the most of the particles of undoped CdS, whereas the Cu doped CdS nanoparticles are monodispersed and isolated from each other. The particles of pure CdS are nearly spherical in shape and a narrow size distribution. The size of CdS nanoparticles ranges from 0.70-4.21nm with an average particle size as ~ 1.91 nm while the Cu doped CdS nanoparticles are in range of 1.77-5.49 nm with an average diameter of ~ 3.07 nm. The corresponding SAED pattern of the CdS and Cu doped CdS nanoparticles respectively shown in the inset of Fig. 2(a) and (b) consists of concentric broad rings which are identified to have cubic structure with diffraction planes corresponding to (1 1 1), (2 2 0) and (3 1 1) for both pure and Cu doped CdS NPs. HRTEM was used to examine the microstructure of the nanoparticles. Fig 2(c) and (d) shows the HRTEM image of the undoped and Cu doped CdS NPs. Both these nanoparticles show diffraction planes (1 1 1), (2 2 0) and (3 1 1) for undoped and Cu doped CdS NPs as shown. The HRTEM of pure and doped CdS nanoparticles shows the presence of the twin structures while the undoped CdS confirms the presence of stacking faults as well with sequence …ABCABABC… by removing a layer C from the perfect-crystal layer sequence …ABCABCABC… as shown in the fig. (c) and (d). These defects play an important role in the optical, electrical and mechanical properties of the nanostructures.

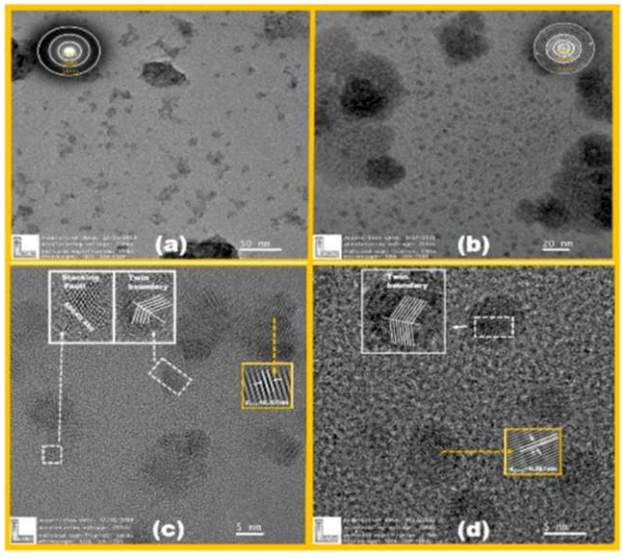

Fig. 2(a) and (b) TEM images, (c) and (d) HR-TEM images of undoped and 3 at% Cu doped CdS QDs

5.2.58 Influence of Swift Heavy Ion Irradiation on Charge Transport Properties of Manganite- Based Thin Films

Alpa Zankat[1] and D.D. Pandya[2]

[1]*Department of Physics, Saurashtra University, Rajkot, 360005, India*

[2]*Human Resource Development Centre, Saurashtra University, Rajkot, 360005, India*

The present work aims to understand the effect of swift heavy ions (SHI) of 100 MeV O irradiation in modifying the structural, microstructural, and transport properties of ~100 nm $La_{0.5}Gd_{0.2}Ca_{0.3}MnO_3$ (LGCMO) films grown on single crystalline (100) Nb: $SrTiO_3$ (SNTO) substrate by pulsed laser deposition (PLD) technique (LGCMO – Pristine) [1]. Here, the irradiation was performed using 15 UD Tandem Accelerator on LGCMO films with different ion fluences ~ 5×10^{11} (LGCMO – 11), 5×10^{12} (LGCMO – 12) and 5×10^{13} ions/cm^2 (LGCMO – 13). The effect of manganite defects created through SHI irradiation at LGCMO–substrate (p–n) interface was investigated via various characterization techniques such as X-ray diffraction (XRD), Atomic force microscopy (AFM), and I-V characteristics. From XRD as evident from Fig.1, there is a decrease in structural strain up for the sample LGCMO-12, while for LGCMO – 13 it gets enhanced due to the irradiation-induced modifications in the crystallinity. The AFM shows improvement in average grain size up to LGCMO-12 but suppression in grain size with increased grain boundary density as well as RMS surface roughness. To understand the transport properties across LGCMO–SNTO p–n interfaces for all films, current-voltage (I–V) characteristics show all the films exhibit non–linear behaviors. The LGCMO–PRI film exhibits backward diode-like behavior while the irradiated films of LGCMO-12 shows the tunnel diode-like behavior and enhancement in conduction across LGCMO–SNTO interface. The higher ion fluence film (LGCMO-13) shows suppression in conduction across the p-n interface in the context of grain size, grain boundary, and interfacial strain, hence, the film exhibits the strongest backward diode characteristics among all the films.

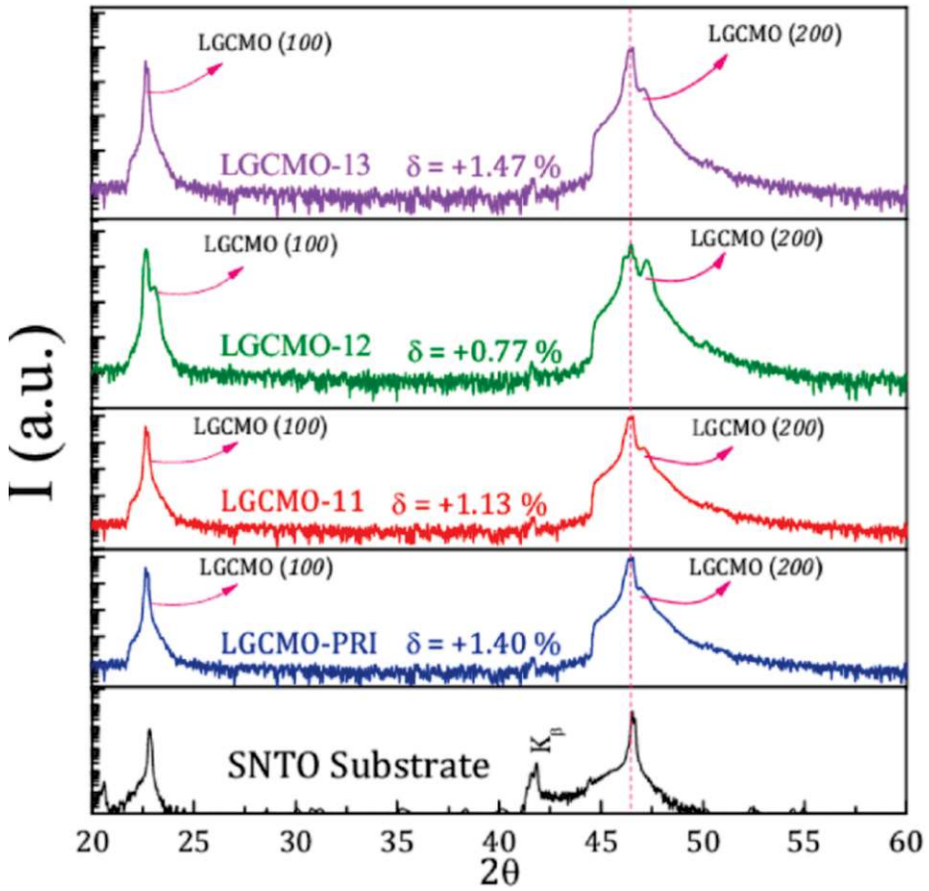

Fig. 1 XRD patterns of SNTO substrate and pristine and irradiated LGCMO/SNTO films.

References:

[1] Alpa Zankat, Keval Gadani, Bhargav Rajyaguru, Khushal Sagapariya, Vivek Pachchigar, M. Ranjan, K. Asokan, P.S. Solanki, N.A. Shah, D.D. Pandya, Physica B 614 (2021) 413013.